

NJC

Accepted Manuscript



This is an *Accepted Manuscript*, which has been through the Royal Society of Chemistry peer review process and has been accepted for publication.

Accepted Manuscripts are published online shortly after acceptance, before technical editing, formatting and proof reading. Using this free service, authors can make their results available to the community, in citable form, before we publish the edited article. We will replace this *Accepted Manuscript* with the edited and formatted *Advance Article* as soon as it is available.

You can find more information about *Accepted Manuscripts* in the [Information for Authors](#).

Please note that technical editing may introduce minor changes to the text and/or graphics, which may alter content. The journal's standard [Terms & Conditions](#) and the [Ethical guidelines](#) still apply. In no event shall the Royal Society of Chemistry be held responsible for any errors or omissions in this *Accepted Manuscript* or any consequences arising from the use of any information it contains.



www.rsc.org/njc

ARTICLE

Magnetic amphiphilic nanocomposites based on silica/carbon for sulphur contaminants oxidation

Cite this: DOI: 10.1039/x0xx00000x

Aline A.S. Oliveira,^a Taís Christofani,^a Ivo F. Teixeira^b, José D. Ardisson^c, Flávia C.C. Moura^{a,*}

Received 00th January 2012,
Accepted 00th January 2012

DOI: 10.1039/x0xx00000x

www.rsc.org/

Silica and carbon based magnetic amphiphilic nanocomposites (MANCs) were synthesized and applied for desulfurization in this work. The structure, composition, magnetic and amphiphilic properties of the resulting MANCs were characterized in detail by physicochemical means such as XRD, elemental analysis, Raman spectroscopy, electron microscopies, thermal analysis, TPR, Mössbauer spectroscopy, magnetization measurements, and contact angle. Different concentrations of Fe and Mo were supported on the surface of silica in order to catalyse the controlled growth of carbon nanotubes and nanofibers by chemical vapor deposition (CVD). The partial coating of hydrophilic silica with hydrophobic carbon nanostructures imparts amphiphilicity, which make the composites a strategic catalyst to promote emulsion formation and to act on the interface. Moreover, during CVD process magnetic species were produced conferring magnetic property which can facilitates the emulsion breakage by a simple magnetic process. Studies on desulfurization reactions catalysed by these nanocomposites were promising and showed that Mo plays an important role on the catalyst efficiency.

Introduction

Amphiphilic materials are defined as chemical species that have in their structure at least two distinct portions: (i) a polar and hydrophilic portion, and (ii) a nonpolar and hydrophobic portion. These materials are capable to promote interaction between media with different polarities, for example, a biphasic system containing water and oil¹. The most common representatives of these amphiphilic materials are surfactant molecules and some polymers. Solid amphiphilic materials began to be recently exploited and are commonly found in the literature as Janus particles². Amphiphilic composites based on different materials have been reported in the literature, such as layered silicates fragments³, chrysotile⁴, vermiculite⁵, molybdenum carbide⁶, magnetic iron oxide⁷, gold nanoparticles⁸, red mud residue¹ and nano alumina⁹.

In this contribution, magnetic amphiphilic nanocomposites (MANCs)¹⁰ were prepared, extensively characterized and applied successfully for diesel desulfurization. This new class of MANCs is based on silica and carbon nanostructures (Figure 1), which are responsible by the amphiphilic character. Iron and specially molybdenum nuclei supported on silica surface play a very important role in the desulfurization process and provide magnetic properties to the MANCs. Remarkably, the same composites that form and stabilize emulsions can be used to separate the phases of a stable emulsion by a simple magnetic process. The magnetic property is essential to facilitate the application of the composites as catalysts.

Experimental

Preparation and Characterization of the MANCs

Silica was impregnated with iron nitrate III ($\text{Fe}(\text{NO}_3)_3 \cdot 9\text{H}_2\text{O}$ - Vetec) and ammonium molybdate ($(\text{NH}_4)_6\text{Mo}_7\text{O}_{24} \cdot 4\text{H}_2\text{O}$ - Rio Lab) in different proportions: a group of samples with 10, 5 and 1 wt% of Fe and another group with Fe10%Mo1%, Fe5%Mo0.5%, and Fe1%Mo0.1%. Composites were named according to the Fe and Mo content, i.e. SiFe10%Mo1%. The impregnated matrix SiO_2 (200 mg) was submitted to a temperature programmed reduction (TPR) with H_2/N_2 (5% H_2) up to 900 °C. After cooling of the system, the samples undergo TPCVD process (Temperature Programmed Chemical Vapor Deposition) with methane heating up to 900 °C. This temperature was held for 60 min. For both experiments, TPR and TPCVD, it was used gas flow of 80 mL min^{-1} and heating rate of 10 °C min^{-1} .

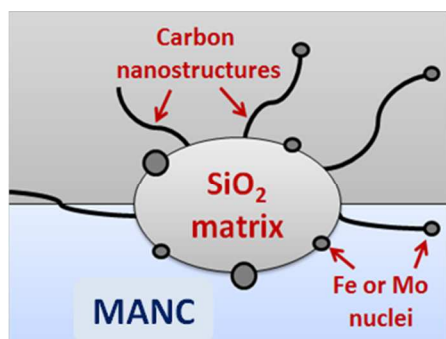


Figure 1. Magnetic amphiphilic nanocomposites (MANCs) based on silica and carbon.

The composites produced were characterized by Temperature Programmed Reduction - TPR (Quanta Chrome CHEMBET-3000), Mössbauer spectroscopy (spectrometer conventional CMTE MA250, constant acceleration, ^{57}Co source in Rh matrix, room temperature), AAS (Hitachi-Z8200 equipment), X-ray diffraction - XRD (diffractometer Rigaku DMAX), magnetization measurements (magnetometer LakeShore 7404 VSM System), thermal analysis - TG (Shimadzu TGA-60, heating rate of $10\text{ }^\circ\text{C min}^{-1}$, air flow of 100 mL min^{-1}), elemental analysis CHN (CHN Perkin-Elmer analyzer), contact angle (goniometer GPX-Digidrop - digitizer of droplets: information about contact angle DGD-DI), Raman spectroscopy (DeltaNu ExamineR, excitation wavelength of 785 nm - red laser), scanning electron microscopy - SEM (microscope SEG - Quanta 200 - SEI) and transmission electron microscopy - TEM (microscope Tecnai G2 200kV - SEI).

Catalytic reactions

The silica/carbon composites prepared were tested initially on the stabilization of reversible emulsions (emulsification/demulsification) between different organic and aqueous phases, i.e. soybean oil/water, mineral oil/water, cyclohexane/ H_2O_2 (aq). The emulsion formation was monitored by optical microscopy (microscope Cole Parmer Instrument, model 41500-5). The ability to emulsify and demulsify of the materials was used to intensify Fenton-like reactions in two-phase systems in which the oxidizing agent (hydrogen peroxide - H_2O_2) is in the aqueous phase and the substrate is in the organic phase¹¹. Emulsifying the system intensifies the contact between the immiscible phases, favoring the reaction. Iron and molybdenum present on the surface of the composites were used to catalyze peroxide activation, characterizing a heterogeneous Fenton-like mechanism.

At first, dibenzothiophene (DBT - Figure S9) was tested as a model sulfur contaminant of crude oil. For each test, it was used 5 mL of dibenzothiophene (Merck) 50 ppm S in cyclohexane. To the organic phase, 10 mg of the material under study was added and the system was left in contact until it reached adsorption equilibrium. After equilibrium, 1 mL of hydrogen peroxide (H_2O_2) (Chemical Dynamics) was added to promote the contaminant oxidation. The contaminants removal was monitored by UV-Vis spectroscopy (Shimadzu UV-2550 with photomultiplier detector R-928) and gas chromatography-mass spectrometry (GC-MS Shimadzu QP2010 - PLUS with electron impact ionization at 70 eV and a nonpolar capillary column RTX® - 5MS).

Tests on the applicability of the materials for sulfur removal in a real sample of diesel S1800 (maximum S concentration 1800 ppm) was performed. In this case, the sulfur content was analyzed by X-ray fluorescence (Shimadzu EDX-800 using ASTM D4294).

Results and discussion

Preparation and characterization of silica/carbon composites

The preparation of the composites was first studied by Temperature Programmed Reduction - TPR (Supplementary Material). The reactions were monitored with respect to the amount of H_2 consumed or released from the composites. In the first step of reaction, Fe and Mo salts are reduced up to Fe^0 and Mo^0 consuming H_2 . In the second step, H_2 is released indicating

the CH_4 decomposition and the deposition of C on the silica surface.

The amphiphilic silica/carbon composites synthesized were extensively characterized in order to obtain information about their metallic and carbon phases. More than that, the structural differences were used to understand their different behaviors as catalysts.

The atomic absorption spectrometry (AAS) was initially used to determine the amount of iron and molybdenum on silica amphiphilic composites synthesized by TPCVD (Table 1). It is observed that the iron content determined by AAS are lower than the theoretical values, since the latter do not take into account the carbon deposits during the CVD process. That is, the final iron content in the composite should be less than the content of silica impregnated matrix.

Table 1. Distribution of iron and molybdenum on the silica nanocomposites, obtained by AAS.

Composite	Iron/%	Molybdenum/%
SFe1%	1.01	0
SFe1%Mo0,1%	0.95	0.36
SFe5%	3.29	0
SFe5%Mo0,5%	3.81	0.75
SFe10%	9.84	0
SFe10%Mo1%	9.07	1.73

It is observed that the percentages obtained by AAS are close to the expected values. The iron content determined by AAS is slightly lower than the theoretical values, since the latter do not take into account the carbon deposited during the CVD process. That is, the final iron content in the composite should be less than the content of the silica matrix only impregnated.

The iron phases formed during the composites synthesis were determined by Mössbauer spectroscopy, as shown in Figure 2.

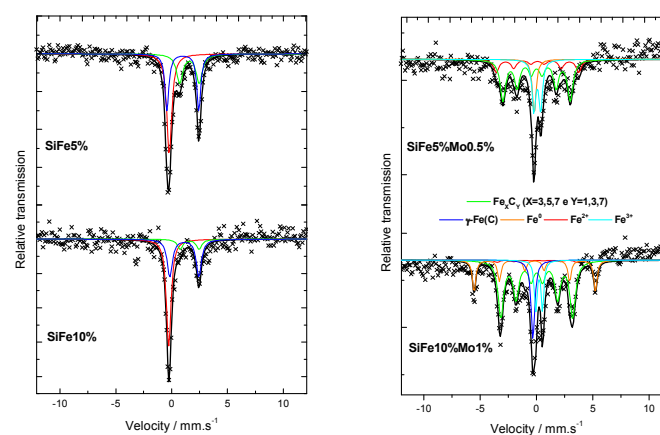


Figure 2. Mössbauer spectra obtained for the amphiphilic materials at room temperature.

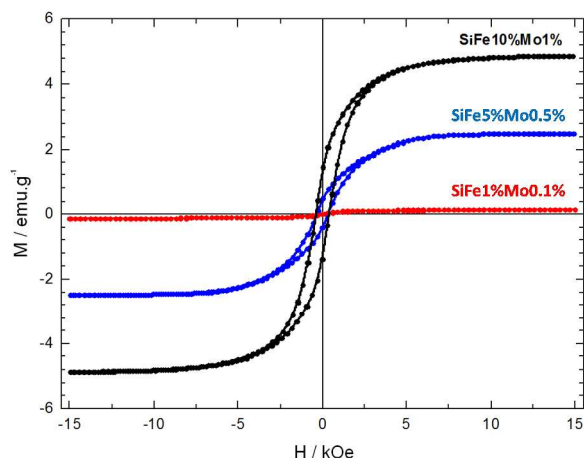
Samples containing 1% of iron did not show significant signal intensity, making it impossible to build Mössbauer spectra due to the low iron content present in these samples. From Mössbauer hyperfine parameters obtained for the materials with 5 and 10% of iron (Supplementary Material) it was possible to determine the composition of each sample related to the iron phase formed. The compositions are expressed in Table 2.

Table 2. Iron phases identified by Mössbauer spectroscopy.

Sample	γ -Fe(C)	Fe ₂ SiO ₄	Fe-Si-C	Fe _x Mo _y	Fe ⁰
SiFe5%	38	34	28	-	-
SiFe10%	12	-	-	67	-
SiFe5%Mo0.5%	50	39	11	-	-
SiFe10%Mo1%	13	-	-	12	20

The phases identified by Mössbauer spectroscopy for the amphiphilic composites are: solid solution of γ -Fe and carbon (γ -Fe(C)), silicate of iron II (Fe₂SiO₄)¹², iron-silicon carbide (Fe-Si-C) also containing Fe²⁺, iron carbide (Fe_xC_y), Fe-Mo alloy (Fe_xMo_y)¹³ with Fe in oxidation state 3+, and metallic iron (Fe⁰). It is observed that in the samples without molybdenum only γ -Fe(C) and Fe₂SiO₄ are formed. The difference between SiFe5% and SiFe10% is due to the higher iron content in the sample SiFe10% that favours the formation of iron carbide. On the other hand, composites containing Mo show mainly Fe_xC_y phase, which is favoured by high concentrations of carbon instead of γ -Fe(C) favoured by lower concentrations of carbon¹⁴. This is in agreement with the carbon content measurements (Figure 4), which shows that samples with Mo have more carbon. Moreover, molybdenum is known as a promoter of the iron carbide formation¹³. Metallic iron is formed only in the sample SiFe10%Mo1% due to its higher iron content.

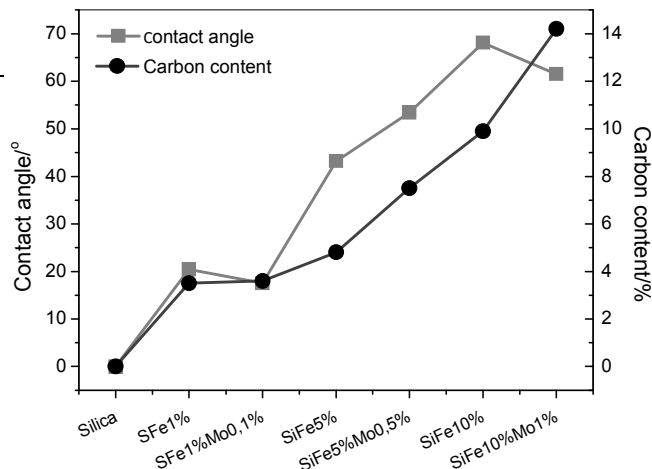
Magnetization measurements were carried out for the series of silica/carbon MANCs. Magnetization curves obtained for materials containing Mo are shown in Figure 3.

**Figure 3.** Magnetization curves obtained for the materials SiFe1Mo0.1%, SiFe5%Mo0.5% and SiFe10%Mo1%.

Although the matrix silica is not magnetic, the composites produced by CVD clearly show magnetization. This magnetic property is due to the reduction of the iron salt impregnated on the matrix during TPR and TPCVD reactions, generating iron magnetic phases, such as Fe⁰ and Fe_xC_y, confirmed by Mössbauer spectroscopy. Materials with 1% Fe showed lower saturation magnetization (<1 emu g⁻¹) due to their low iron concentration. However, during bench tests it was observed that the materials SiFe1% and SiFe1%Mo0.1% are attracted by a magnet. As expected, the saturation magnetization increases with the Fe content. Magnetic susceptibility results show that composites can be recovered from the reaction medium by the application of a magnetic field as has been proven experimentally^{15,16}.

The amphiphilicity of the materials can be controlled by their carbon content: the higher the carbon content, the greater

hydrophobic character. The relation between carbon content and contact angle can be seen in Figure 4.

**Figure 4.** Contact angle measurements and carbon content for the amphiphilic silica/carbon composites.

It can be observed that the increase in the contact angle is directly related to the carbon content of the composites. Pure silica is very hydrophilic, showing contact angle of approximately 0°. This matrix only impregnated with Fe and Mo salts, without carbon, is also completely hydrophilic (contact angle near 0°). On the other hand, the composites prepared by CVD reaction of silica, Fe/Mo and methane present higher contact angles, i.e. 20° for SiFe1%, 18° for SiFe1%Mo0.1%, 43° for SiFe5%, 53° for SiFe5%Mo0.5%, 68° for SiFe10% and 62° for SiFe10%Mo1%.

CHN results show that the higher the Fe and Mo content, the greater the amount of carbon deposited, as shown in Supplementary Material. Several studies in the literature show that molybdenum acts as co-catalyst in the presence of iron to catalyze carbon deposition in organized forms^{13,17,18}, what is in agreement with the obtained results.

It is observed that SiFe1%Mo0.1% and SiFe10%Mo1% present lower contact angles than SiFe1% and SiFe10%, respectively, despite having higher carbon content. This can be due to the effect of Mo, which clearly inhibits the formation of Fe₂SiO₄ phase, favoring the formation of hydrophilic phases exposed on the silica surface, as shown by Mössbauer spectroscopy. These metal hydrophilic phases were confirmed by TGA (Supplementary Material), which show a weight gain related to oxidation of metallic phases (350-450°C) before the carbon oxidation (500-700°C)¹⁹. Despite having exposed metallic phases the sample SiFe5%Mo0.5% do not show the same behavior that may be related to the fact that this sample has much more organized carbon phases (Figure 5) than the other samples.

In order to characterize carbon deposits formed on the materials surface with different contents of iron and molybdenum, Raman spectra were obtained (Figure 5).

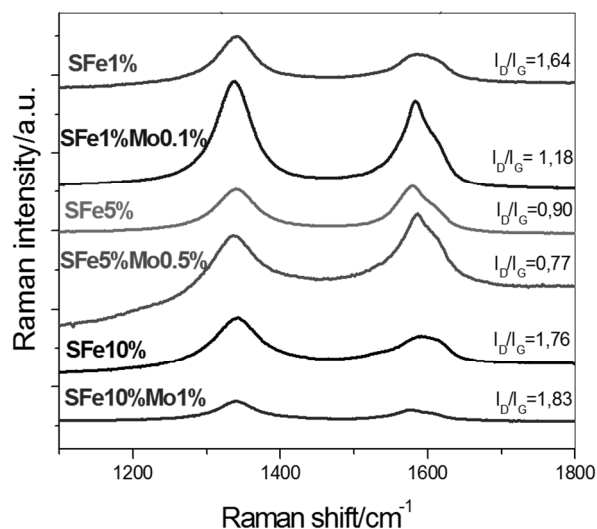


Figure 5. Raman spectra obtained for the amphiphilic composites.

Raman spectra in **Figure 5** shows intense D and G bands at about 1340 and 1580 cm^{-1} , respectively. The presence of the D band suggests the formation of defective carbon structures, such as defective CNT. On the other hand, G band represents the formation of organized carbon structures, such as graphite and carbon nanotubes (CNT)²⁰. It is observed that the G band appears asymmetric for all materials, especially for SiFe1%Mo0.1%, SiFe5%Mo0.5% and SiFe5%, which may be associated to the presence of single-walled carbon nanotubes (SWCNT)²¹. All samples showed a high ratio I_D/I_G , which suggests that the carbon filaments produced are likely agglomerated and/or twisted and with high amount of defects. However, it might be a desirable feature as some studies demonstrate that defects in carbon nanostructures significantly increase their catalytic activities^{22, 23}.

The morphology of the silica/carbon composites was investigated by SEM. Images obtained for the amphiphilic materials (**Figure 6**) showed that the matrix silica remains with the same morphology even after the synthesis steps. On the surface of the matrix, supported metal nanoparticles are dispersed all over the material. Figure 6 also shows agglomerates of carbon filaments on MANCs surface.

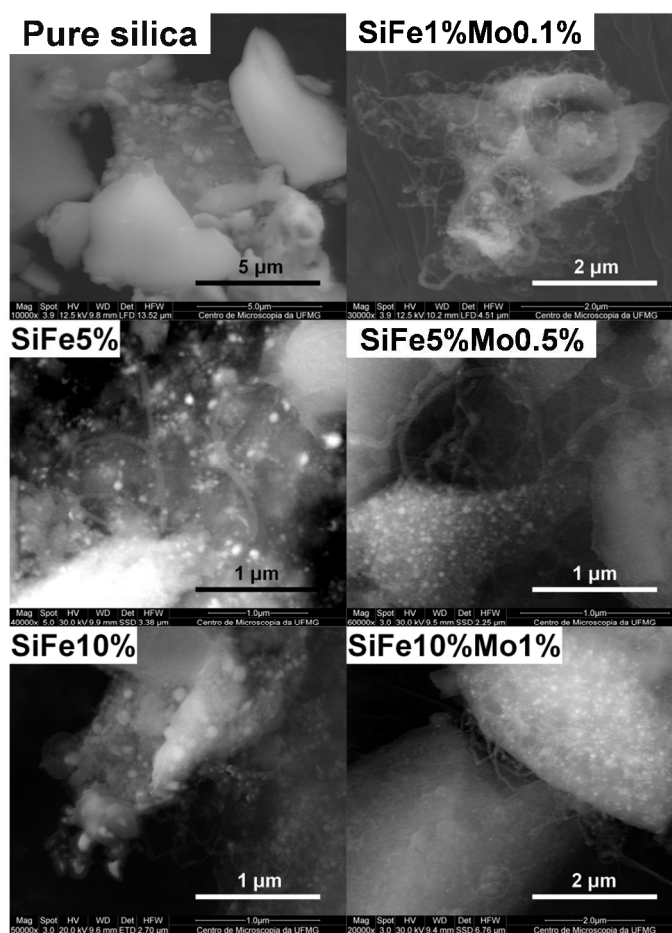


Figure 6. SEM images obtained for pure silica and composites, showing filaments and metal nanoparticles.

In order to better observe the nanometric structures, TEM images were obtained for SiFe10% and SiFe10%Mo1% (**Figure 7**). Metal nanoparticles with diameters between 10 and 50 nm encapsulated by carbon can be observed, and also, carbon nanotubes with diameters between 5 and 50 nm. These nanotubes are present in agglomerates, often twisted, which characterizes regions of defects, this is in agreement with the intensity of Raman D band and I_D/I_G ratios (see **Figure 5**).

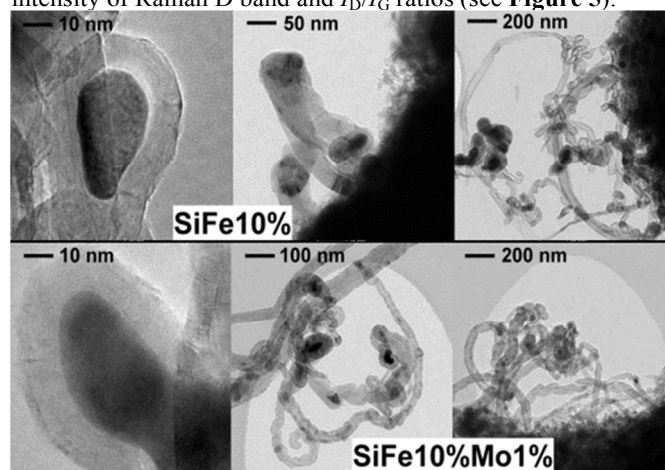


Figure 7. Images obtained by TEM for composites with 10% of iron, showing coated metallic nanoparticles and several filaments.

Catalytic reactions

In order to gauge the effectiveness of the amphiphilic silica/carbon composites, as promoters of reactions in biphasic systems, MANCs were tested first as emulsifiers. The emulsion formation between immiscible phases, such as water/cyclohexane, water/soybean oil or water/decalin, is essential for the reaction yield. Amphiphilic composites favor the formation and stabilization of organic droplets dispersed in aqueous phase because they remain on the interface oil/water, avoiding droplets coalescence (Figure 8).

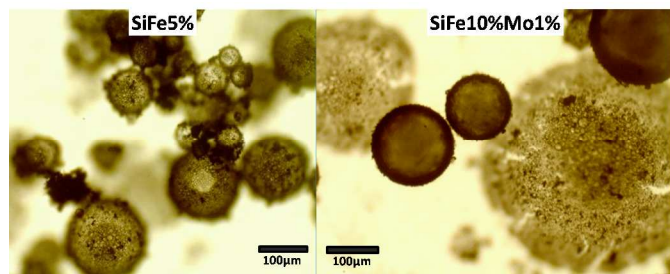


Figure 8. Microscopic images of cyclohexane/water emulsions stabilized by the amphiphilic composites.

As the materials can form stable emulsions between two immiscible phases, they were tested in biphasic oxidation reactions of dibenzothiophene (DBT). Figure 9 summarizes how these composites act in this reaction. In the first step MANCs promote emulsion formation, increasing the interface between organic and aqueous phases.

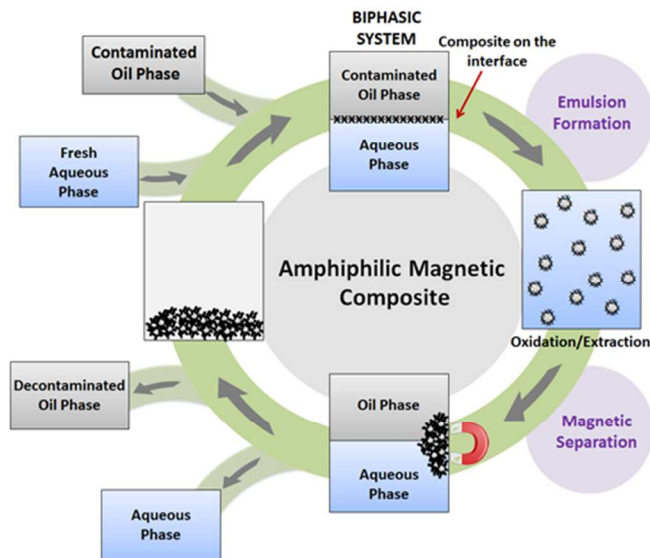


Figure 9. Scheme of silica/carbon composites application in desulfurization reactions.

Hydrogen peroxide is activated by Fe and Mo species on the surface of the composites in a heterogeneous Fenton-like mechanism, forming highly oxidizing hydroxyl groups ($\bullet\text{OH}$)²⁴ on the interface of the immiscible phases. By intensifying the interface, the composites facilitate the contact between $\bullet\text{OH}$ radicals and DBT molecules. The oxidized contaminant is extracted to the aqueous phase by polarity. After reaction, the amphiphilic silica/carbon composites located on the interface can be attracted by an external magnet. The removal of the materials from the interface destabilizes the emulsion formed

and the phases are separated. The catalysts can then be removed magnetically from the system and reused for several times. The catalysts were reused in at least three consecutive tests of DBT oxidation and showed similar activity.

The dibenzothiophene oxidation reactions were carried out using solutions containing 50 ppm of DBT, in order to test the composites under ultra-desulfurization conditions. DBT concentration in organic phase (cyclohexane) was monitored by UV-Vis spectroscopy (Figure 10).

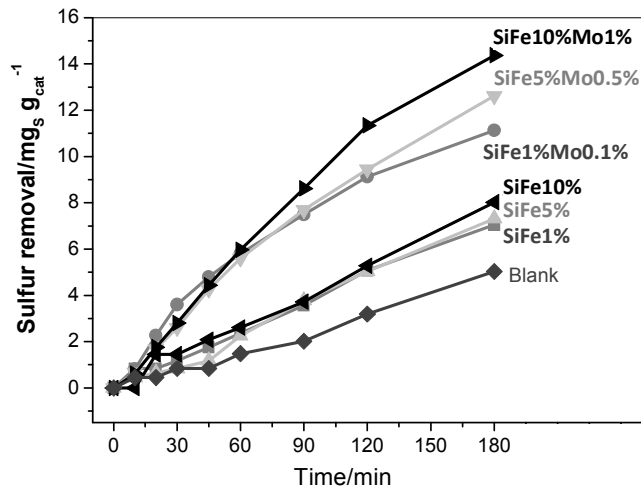


Figure 10. DBT removal in the presence of amphiphilic materials (5 mL DBT 50 ppm S in cyclohexane, 1 mL H_2O_2 , 10 mg catalyst).

It is important to note that the same trend is observed for both groups: (i) composites with Mo and (ii) composites without Mo. In each group, the catalysts are more efficient as more metal they have. Furthermore, the materials containing molybdenum are more efficient to remove DBT, probably because Mo nuclei are also active^{25,26} for peroxide activation, but extremely resistant to sulfur poisoning^{27,28}. Therefore, the efficiency of the catalyst depends on the amount of carbon and the availability of metal particles present on their surface to promote the H_2O_2 activation²⁹. From Mössbauer results, we observe that materials containing Mo present iron carbide in their composition, which might be associated with its activity. Results of dibenzothiophene oxidation (Figure 10) show that the silica/carbon composites prepared can be applied as catalysts, since the sulphur removal is much higher in the presence of these composites, especially those containing Mo. The best catalyst (SiFe10%Mo1%) reaches 15 $\text{mgS g}_{\text{cat}}^{-1}$, compared to 4 mg S for the blank experiment, this is a relatively good result for deep oxididesulfurization compared to other results from the literature^{30,31}.

The oxidation of sulphur was also tested for real contaminated diesel samples. In these experiments, catalysts containing molybdenum presented again higher efficiency in the desulfurization (Figure 11).

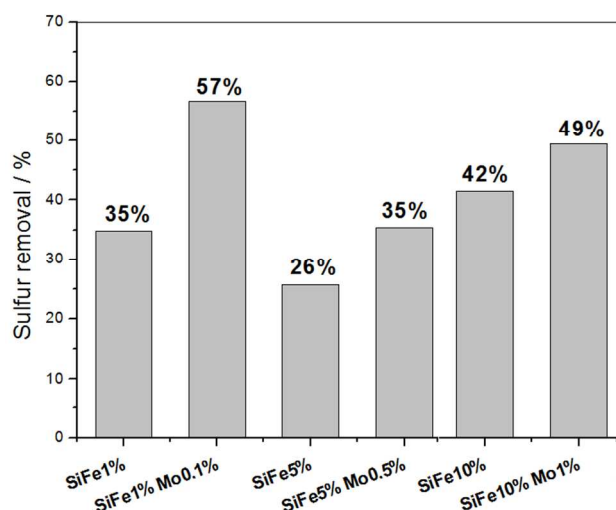


Figure 11. Removal of sulfur in diesel S1800 in the presence of the composites (5 mL diesel S1800, 1 mL H₂O₂, 10 mg catalyst).

Diesel is a complex matrix with different physico-chemical properties compared to the model solution and contains a variety of S-molecules, including BT, DBT and 4,6 DMDBT. These molecules can be even more difficult to be oxidized, due mainly to steric effects³². However, it is observed that the percentage reduction on the sulfur content in diesel (**Figure 11**) is comparable to the reduction obtained in experiments with model solutions of DBT in cyclohexane (**Figure 10**), approximately 60%.

Experiments of DBT oxidation in the presence of the composite SiFe10%Mo1% were monitored by GC-MS in order to identify the oxidation products.

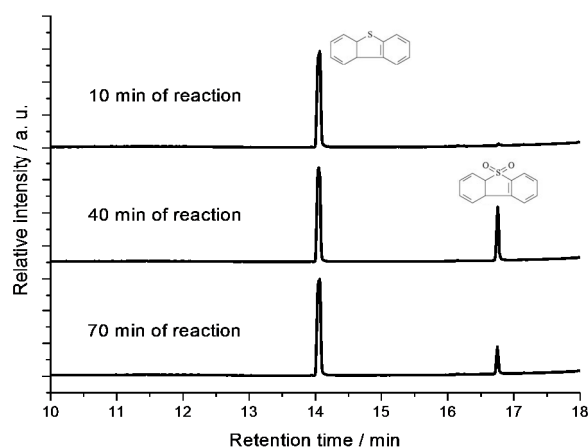
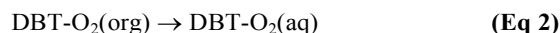
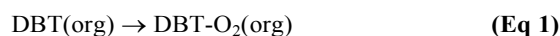


Figure 12. Chromatograms of the organic phase of DBT oxidation reaction, obtained by GC-MS.

Chromatograms of **Figure 12** show that at the beginning of the reaction only one peak related to DBT can be observed, with retention time of 14 min. During the reaction in the presence of the silica/carbon catalyst, a new peak appeared with retention time of 16.8 min, probably related to a reaction product. After 14 min, the area of DBT peak decreased slightly, while the second peak area, referring to the reaction product, increases over time and later it starts to decrease. Probably because it begins to be extracted by the aqueous phase, due to its higher hydrophilicity. These peaks were identified by mass

spectrometry (**Figure S8**) as dibenzothiophene ($m/z = 184$) and dibenzothiophene sulfone ($m/z = 216$), respectively.

The oxidized product of dibenzothiophene first appears in the organic phase due to its intermediate polarity and low concentration (Eq. 1). Increasing the reaction time, the peak referent to the oxidized product disappears from organic phase, suggesting that the dibenzothiophene sulfone produced has passed into the aqueous phase (Eq. 2). Thus, the organic phase (fuel) has the concentration of S containing contaminants decreasing over time. This reaction mechanism is very well established and has been reported by different research groups³³⁻³⁷.



The detailed mechanism proposed for the biphasic desulfurization catalysed by the composites was depicted in **Figure 13**.

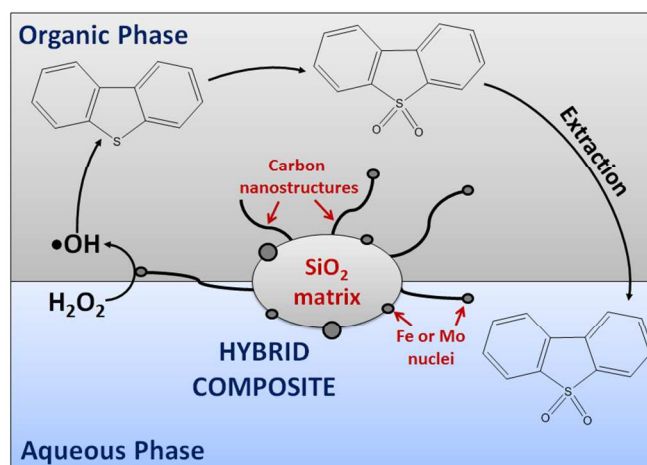
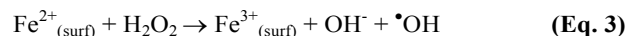


Figure 13. Mechanism of desulfurization catalysed by the amphiphilic composites.

In the first step of the mechanism, the composites act increasing the interface between diesel and aqueous phases, forming an emulsion with high interface. Then, hydrogen peroxide is activated by Fe and Mo species on the surface of the composites in a heterogeneous Fenton-like mechanism, forming hydroxyl groups ($\bullet\text{OH}$) (Eq 3). $\bullet\text{OH}$ radicals rapidly react with the sulphur molecule and initiate the oxidation process or either can react with other H₂O₂ molecules to form hydroperoxyl radicals, HOO \bullet , highly oxidizing peracid species which are also capable to oxidize the DTB on the interface of the immiscible phases (Eq. 4).



By intensifying the interface, the composites facilitate the contact between the radicals and S-molecules. Consequently, the radicals can initiate the selective oxidation of the S-

contaminants present in the organic phase, and finally, the oxidized S-contaminant is extracted by the aqueous phase due to its increased polarity. At the end of reaction, the composites located on the interface can be attracted by an external magnet, which destabilizes the emulsion formed and the phases are separated.

The efficiency obtained by the silica nanocomposites in this study is comparable to recent papers of other researcher groups. Madeira *et al*³⁸ obtained 60% S removal via biodesulfurization, same as Vargas *et al*³⁹ with experiments of photocatalysis. Some studies show lower activities, including Bhasarkar *et al*⁴⁰ that obtained ~50% via oxidative desulfurization assisted by phase transfer agent and ultrasound and Mohamed *et al*⁴¹ that achieved 18% of sulfur reduction in hexane.

Conclusions

Magnetic amphiphilic nanocomposites (MANCs) based on silica and carbon were produced and tested for desulfurization. Fe and Mo supported on the surface of silica were used to catalyze carbon deposition by the chemical vapor deposition method. Characterization results showed that the iron phases were reduced to confer magnetic property to the composites. Carbon content of the materials with different Fe/Mo ratios varies from 3 to 14% mainly as carbon nanotubes and nanofibers, which in turn can tune the amphiphilicity. It was demonstrated that the MANCs can interact at the same time with aqueous and organic phases and increase the interface of biphasic systems, promoting the formation of stable emulsions. Studies on the use of the composites as catalysts for biphasic desulfurization reactions showed that these composites, especially those containing Mo, are promising for the removal of S compounds from petroleum and its derivatives. Further, Mo plays an important role in the desulfurization process, since composites containing Mo in all concentrations tested showed superior efficiencies. The influence of Mo is likely associated with its activity for H₂O₂ activation and resistance to sulfur poisoning. At the end of the process, the catalysts are easily removed by magnetic separation and can be reused. These MANCs exhibit great potential to be used as catalysts for different other biphasic reactions and new experiments are underway.

Acknowledgements

The authors would like to acknowledge PETROBRAS, CAPES, CNPq and FAPEMIG for financial support and also the Center of Microscopy at the Universidade Federal de Minas Gerais (<http://www.microscopia.ufmg.br>) for providing the equipment and technical support for experiments involving electron microscopy.

Notes and references

^a Departamento de Química, ICEX, Universidade Federal de Minas Gerais, Av. Antônio Carlos 6627, Belo Horizonte, Brazil. Fax: 55 31 34095700, Tel: 55 31 34097556. flaviamoura@ufmg.br

^b Department of Chemistry, University of Oxford, OX1 3QR, UK.

^c Laboratório de Física Aplicada, CDTN. Belo Horizonte, MG, Brazil.

1. A. A. S. Oliveira, I. F. Teixeira, L. P. Ribeiro, J. C. Tristao, A. Dias and R. M. Lago, *Journal of the Brazilian Chemical Society*, 2010, **21**, 2184-2188.
2. P. G. de Gennes, *Reviews of Modern Physics*, 1992, **64**, 645-648.
3. A. D. Purceno, A. P. C. Teixeira, N. J. d. Souza, L. E. Fernandez-Outon, J. D. Ardisson and R. M. Lago, *J. Colloid Interface Sci.*, 2012, **379**, 84-88.
4. A. P. C. Teixeira, A. D. Purceno, C. C. A. de Paula, J. C. C. da Silva, J. D. Ardisson and R. M. Lago, *Journal of Hazardous Materials*, 2013, **248-249**, 295-302.
5. A. P. C. Teixeira, A. D. Purceno, A. S. Barros, B. R. S. Lemos, J. D. Ardisson, W. A. A. Macedo, E. C. O. Nassor, C. C. Amorim, F. C. C. Moura, M. G. Hernandez-Terrones, F. M. Portela and R. M. Lago, *Catal. Today*, Ahead of Print.
6. R. V. F. Mambri, T. L.; Dias, A.; Oliveira, L. C.; Araujo, M. H.; Moura, F.C., *J. Hazard. Mater.*, 2012, **241-242**, 73-81.
7. W. F. Souza, M. C. Pereira and L. C. A. Oliveira, *Fuel*, 2012, **96**, 604-607.
8. R. Tarnawski and M. Ulbricht, *Colloids and Surfaces A: Physicochemical and Engineering Aspects*, 2011, **374**, 13-21.
9. A. A. S. Oliveira, I. F. Teixeira, L. P. Ribeiro, E. Lorençon, J. D. Ardisson, L. Fernandez-Outon, W. A. A. Macedo and F. C. C. Moura, *Applied Catalysis A: General*, 2013, **456**, 126-134.
10. I. F. Teixeira, A. A. d. S. Oliveira, T. Christofani and F. C. C. Moura, *Journal of Materials Chemistry A*, 2013, **1**, 10203-10208.
11. X. Jiang, H. Li, W. Zhu, L. He, H. Shu and J. Lu, *Fuel*, 2009, **88**, 431-436.
12. W. Kündig, J. A. Cape, R. H. Lindquist and G. Constabaris, *Journal of Applied Physics*, 1967, **38**, 947-948.
13. A. P. C. Teixeira, B. R. S. Lemos, L. A. Magalhaes, J. D. Ardisson, R. M. Lago, C. A. Furtado and A. P. Santos, *J. Nanosci. Nanotechnol.*, 2012, **12**, 2661-2667.
14. H. Ohtani, M. Hasebe and T. Nishizawa, *Trans. Iron Steel Inst. Jpn.*, 1984, **24**, 857-864.
15. R. Gerber, 1994, pp. 165-220.
16. E. Karimi, I. F. Teixeira, A. Gomez, E. de Resende, C. Gissane, J. Leitch, V. Jollet, I. Aigner, F. Berruti, C. Briens, P. Fransham, B. Hoff, N. Schrier, R. M. Lago, S. W. Kycia, R. Heck and M. Schlaf, *Applied Catalysis B: Environmental*, 2014, **145**, 187-196.
17. Y. Li, J. Liu, Y. Wang and Z. L. Wang, *Chem. Mater.*, 2001, **13**, 1008-1014.
18. H. Yoshida, T. Shimizu, T. Uchiyama, H. Kohno, Y. Homma and S. Takeda, *Nano Letters*, 2009, **9**, 3810-3815.
19. I. F. Teixeira, T. P. V. Medeiros, P. E. Freitas, M. G. Rosmaninho, J. D. Ardisson and R. M. Lago, *Fuel*, 2014, **124**, 7-13.
20. M. Nippe, R. S. Khnayzer, J. A. Panetier, D. Z. Zee, B. S. Olaiya, M. Head-Gordon, C. J. Chang, F. N. Castellano and J. R. Long, *Chemical Science*, 2013, **4**, 3934-3945.
21. A. Jorio, M. A. Pimenta, A. G. Souza, R. Saito, G. Dresselhaus and M. S. Dresselhaus, *New Journal of Physics*, 2003, **5**.
22. S. Song and S. Jiang, *Applied Catalysis B: Environmental*, 2012, **117-118**, 346-350.
23. Y. Cao, H. Yu, J. Tan, F. Peng, H. Wang, J. Li, W. Zheng and N.-B. Wong, *Carbon*, 2013, **57**, 433-442.

24. H. S. Oliveira, L. C. A. Oliveira, M. C. Pereira, J. D. Ardisson, P. P. Souza, P. O. Patricio and F. C. C. Moura, *New Journal of Chemistry*, 2015.
25. V. V. D. N. Prasad, K.-E. Jeong, H.-J. Chae, C.-U. Kim and S.-Y. Jeong, *Catalysis Communications*, 2008, **9**, 1966-1969.
26. A. Chica, A. Corma and M. E. Domine, *J. Catal.*, 2006, **242**, 299-308.
27. B. R. Greenhalgh, S. M. Kuznicki and A. E. Nelson, *Applied Catalysis A: General*, 2007, **327**, 189-196.
28. B. H. Danziger, *Industrial & Engineering Chemistry*, 1955, **47**, 1495-1500.
29. D. A. S. Costa, A. A. S. Oliveira, P. P. de Souza, K. Sapag and F. C. C. Moura, *New Journal of Chemistry*, 2015, **39**, 1438-1444.
30. Y. Shen, T. Sun, X. Liu and J. Jia, *RSC Advances*, 2012, **2**, 4189-4197.
31. A. A. S. Oliveira, D. A. S. Costa, I. F. Teixeira and F. C. C. Moura, *Applied Catalysis B: Environmental*, 2015, **162**, 475-482.
32. C. Komintarachat and W. Trakarnpruk, *Industrial & Engineering Chemistry Research*, 2006, **45**, 1853-1856.
33. A. Treiber, P. M. Dansette, H. El Amri, J.-P. Girault, D. Ginderow, J.-P. Mornon and D. Mansuy, *Journal of the American Chemical Society*, 1997, **119**, 1565-1571.
34. K. N. Brown and J. H. Espenson, *Inorganic Chemistry*, 1996, **35**, 7211-7216.
35. M. R. Maurya, A. Arya, A. Kumar, M. L. Kuznetsov, F. Avecilla and J. Costa Pessoa, *Inorganic Chemistry*, 2010, **49**, 6586-6600.
36. L. Kong, G. Li and X. Wang, *Catalysis Today*, 2004, **93-95**, 341-345.
37. K. Yazu, Y. Yamamoto, T. Furuya, K. Miki and K. Ukegawa, *Energy & Fuels*, 2001, **15**, 1535-1536.
38. L. da Silva Madeira, V. S. Ferreira-Leitão and E. P. da Silva Bon, *Chemosphere*, 2008, **71**, 189-194.
39. R. Vargas and O. Núñez, *Journal of Molecular Catalysis A: Chemical*, 2008, **294**, 74-81.
40. J. B. Bhasarkar, S. Chakma and V. S. Moholkar, *Ultrasonics Sonochemistry*, 2015, **24**, 98-106.
41. M. E.-S. Mohamed, Z. Al-Yacoub and J. Vedakumar, *Frontiers in Microbiology*, 2015, **6**.